This is an open access article published under an ACS AuthorChoice License, which permits copying and redistribution of the article or any adaptations for non-commercial purposes.

ACS OMEGA

Article

Cite This: ACS Omega 2018, 3, 7904−7910

Transformation of Solid Waste into Nanoporous Carbon via Carbothermic Reduction

Chang Hyun Kim,[†,‡] Jae-Hyun Kim,[†,‡] and Seung-Mo Lee*[,†,‡]

[†]Department of Nanomechanics, Korea Institute of Machinery and Materials (KIMM), 156 Gajeongbuk-ro, Yuseong-gu, Daejeon 34103, South Korea

[‡]Nano Mechatronics, Korea University of Science and Technology (UST), 217 Gajeong-ro, Yuseong-gu, Daejeon 34113, South Korea

Supporting Information

ABSTRACT: Continuous population growth and rapid urbanization will outpace the global capacity of solid-waste disposal. Although pyrolysis, in the waste management sector, has been regarded as a savior to bring potential returns, it has struggled against high operation costs. Here, we found that simple pyrolysis of properly mixed wastes [e.g., organic wastes (C) + metal wastes in the form of metal oxides (M_xO_y)] can bring about the carbothermic reduction [$C(s) + M_xO_y(s) \rightarrow C'(s) + M(s) + CO(g)$] caused by the thermodynamic reducibility of metal oxide. This process consequently produced not only nanoporous carbon powder usable for energy storage devices but also nanoporous carbon fully decorated with magnetic nanoparticles useful for magnetic applications. We believe that the carbothermic reduction process, historically used for metal refining, could be a promising alternative to resolve the long-pending issues of the conventional pyrolysis approach as well as to produce useful nanoporous carbon with ease. Our method could be a simple and effective way to transform ubiquitous solid waste into useful resources in the form of nanoporous carbon.

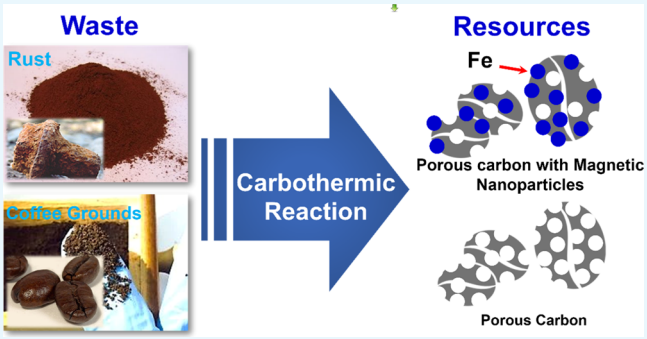

INTRODUCTION

Solid waste, a byproduct of civilization, is any unwanted and unusable substance which is discarded after primary use. In the past century, as the world's population has grown and become affluent, waste production has increased 10-fold. It will double again by 2025.[1] Even now, waste is being endlessly generated faster than other environmental pollutants, including greenhouse gases, and is escaping into the environment. Discarded materials have been collected, some have been recycled or composted, and most have been landfilled or incinerated with negligible energy recovery.[2] Recently, in the waste management sector, pyrolysis (the thermochemical decomposition of organic materials) is getting great attention for its potential returns ("waste to fuel").[3−9] However, pyrolysis is complex and requires striking operation and investment costs. Furthermore, produced gases and ashes contain high heavy metal content, which are regarded as dangerous wastes.[10] Hence, virtually, most of the wastes have been eventually discarded by conventional incineration because of technical, regulatory, reputational, and financial risks.[10] Therefore, it is still highly demanding to make a breakthrough to overcome technological and economical impediments faced by the typical pyrolysis process. Herein, we demonstrate that the carbothermic reduction process, typically used for extraction of metals from ores in nature, could be a promising alternative to resolve the long-pending issues of the conventional pyrolysis approach toward waste treatment. We show that simple pyrolysis of properly mixed wastes [e.g., organic wastes (C) + metal wastes in the form of metal oxides (M_xO_y)] can bring about the carbothermic reduction [$C(s) + M_xO_y(s) \rightarrow C'(s) + M(s) + CO(g)$] caused by the thermodynamic reducibility of metal oxide reported by Ellingham.[11] This process was observed to consequently produce nanoporous carbon powder with insufficient yet but potentially increasable electrochemical performances or nanoporous carbon fully decorated with superparamagnetic metal nanoparticles certainly useful for high-value biomedical[12,13] and environmental applications.[14]

RESULTS AND DISCUSSION

Coffee is one of the largest agricultural products, which is mainly used for beverages. According to the International Coffee Organization, the total world's coffee production in 2017 was 15 893 × 10^4 bags (60 kg/bag) and each year approximately 8 million metric tons of coffee is being produced globally.[15] Recently, average coffee consumption in South Korea has significantly grown at an annual rate of 7%. The

Received: June 7, 2018
Accepted: June 26, 2018
Published: July 17, 2018

© 2018 American Chemical Society

DOI: 10.1021/acsomega.8b01280
ACS Omega 2018, 3, 7904−7910

amount of coffee bean waste (CBW, i.e., the spent coffee grounds, the solid residue remaining after brewing) has increased steadily. Most of the CBW has been discarded with negligible regard for future use as a solid waste, which is creating great disposal costs and waiting for a proper way for waste treatment. For this reason, in this study, we employed the ubiquitously existing coffee waste in South Korea. As a source of metal oxide, we selected Fe_2O_3 for production of nanoporous carbon, taking into account the fact that Fe_2O_3 is naturally occurring and omnipresent rust.

Production of Nanoporous Carbon via Carbothermic Reduction. Historically, carbothermic reduction, one of the oldest metallurgical processes, has been widely utilized to smelt various metals by removing oxygen from metal oxides. With increasing industrial applications, the mechanism of this reaction was a subject of numerous studies. In particular, Ellingham constructed a diagram to predict the equilibrium temperature between a metal, its oxides, and oxygen and to evaluate the ease of the reduction of metal oxides.[11] Typically, this involves heating the oxide together with carbon as the reducing agent to drive off other elements such as gases and slag and finally to leave pure metal [$MO(s) + C(s) \rightarrow M(s) + CO(g)$]. We paid special attention to this conventional chemical formula and thought in a totally different way. We assumed that instead of carbon, metal oxide can also be used as a sacrificial agent [i.e., $C(s) + MO(s) \rightarrow C'(s) + M(g \text{ or } s) + CO(g)$] in order to activate carbon and at the same time produce pure metal once carbon is not decomposed and metal oxide is fully reduced, finally evaporating in a certain high temperature range.[16,17] It was anticipated that the reaction of metal oxide can create numerous pores on the surface of carbon and finally produce nanoporous carbon fully decorated with metal nanoparticles depending on the melting point of the metal and processing temperature, so long as the adhesion between the metal oxide and the carbon is strong enough. According to the literature, the Fe_2O_3 in the mixture (c-CBW/Fe_2O_3) was thought to be reducible at a relatively low temperature (~900 °C) than other metal oxides [likely, $C(s) + Fe_2O_3(s) \rightarrow C' + CO(g) + Fe(s)$, see Figure S1].[18] Because the melting temperature of Fe is around 1538 °C higher than our processing temperature, it was expected that Fe in the form of nanoparticles remains on the porosified carbon surface. On the basis of this scenario, as depicted in Figure 1, first, we annealed the collected CBW for removal of inherent impurities such as water, which led to carbonization (c-CBW). After mixing with rust (c-CBW/Fe_2O_3), pyrolysis was carried out, which resulted in nanoporous carbon particles fully decorated with iron nanoparticles [porous carbon (PC)/Fe]. The iron particles were able to be easily removed by washing with acidic solution, which resulted in pure PC. The effect of the carbothermic reduction on the physical and chemical properties of the CBW is quite notable, as can be recognized from various analysis results (Figure 2).

Thermogravimetric analysis (TGA) indicated that in the region of RT < T < ~350 °C, water and other impurities in the CBW are evaporated, thereby causing a significant decrease in weight. The carbonization temperature was observed to be less critical to the graphitic nature of the c-CBW, as long as it is over ~350 °C (Figure S2). The carbothermic reduction in c-CBW/Fe_2O_3 likely occurred at ~850 °C in consideration of the slight decrease in weight (Figure 2a). The Raman spectra (Figure 2b) exhibited two peaks at around 1320 and 1590 cm^{-1}, which were assigned to the characteristic defective D band and graphitic G band of carbon materials, respectively.[19] The relative intensity ratio of D/G implies the degree of structural disorder with respect to a perfect graphitic structure. Taking into account the less noticeable alteration in D/G ratio before and after carbothermic reduction, the reduction likely did not cause any significant chemical changes except morphological changes. However, X-ray diffraction (XRD) results exhibited that the Fe_2O_3 nanoparticles covering c-CBW are completely reduced to Fe via carbothermic reduction according to our expectation, as can be recognized from the spectra of c-CBW/Fe_2O_3 and PC/Fe (Figure 2c). Therefore, the solid-state etching of carbon by the carbothermic reduction led to the alteration in the morphology of the c-CBW, as can be noticed from Figure 3.

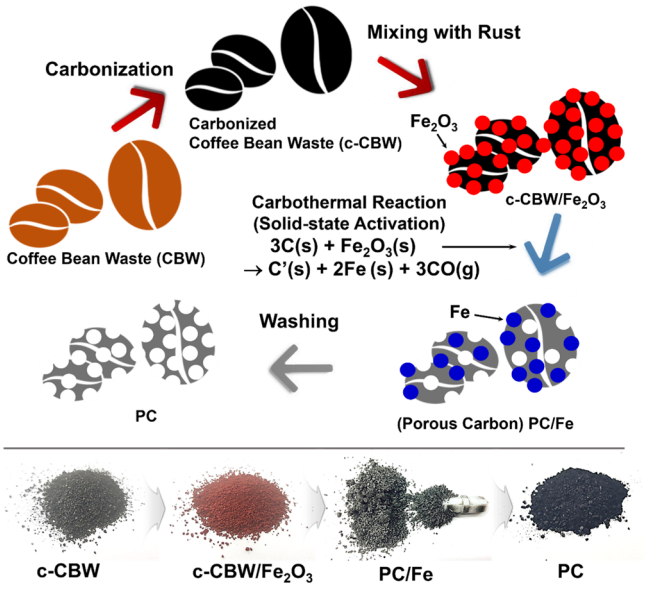

Figure 1. Schematic showing the preparation procedure for multifunctional nanoporous carbon powder. Using carbothermic reduction, we transformed residential solid waste (CBW and rust) into another resource such as nanoporous carbon with/without magnetic nanoparticles. In the practical application of our method, the carbonization step, that is, CBW → c-CBW, is not required. For the control experiment in this work, we included the carbonization step. Therefore, mixing CBW with rust and subsequent pyrolysis can lead to the same results. The figure at the bottom shows real photographs of the produced materials.

Elemental Analysis and Microstructure. The initial annealing was observed to bring about less remarkable changes in the morphology of the raw CBW powder. Thus, the morphological differences between CBW and carbonized CBW (c-CBW) were less recognizable (Figure 3a). The rigorous mixing with iron oxide powder with a particle size of few tens of nanometers [c-CBW/Fe_2O_3 with a weight ratio of 4(Fe_2O_3):1(CBW)] resulted in a serious change in color (from black to red) and nearly uniform coating (Figure 3b). The annealing of the mixture c-CBW/Fe_2O_3 at a temperature of ~900 °C led to significant morphological changes, likely because of the phase transformation of Fe_2O_3 that occurred during carbothermic reduction (Figure 3c). The resulting PC decorated with Fe particles (PC/Fe) was thinner and rougher than the CBW. After removing Fe nanoparticles by washing, the PC became even more porous (Figure 3d). Regarding the elemental change and distribution of the rust (Fe_2O_3) and iron particles, further studies were performed using transmission

DOI: 10.1021/acsomega.8b01280
ACS Omega 2018, 3, 7904−7910

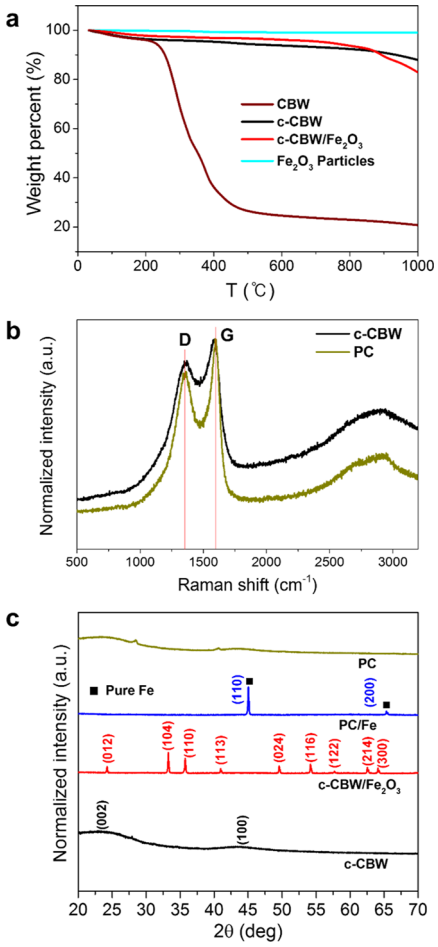

Figure 2. Chemical and physical analysis. (a) TGA results. (b) Raman spectra showing changes in the relative intensity ratio of G to D bands (D/G ratio). (c) XRD spectra showing crystal phase changes at each step of the carbothermic reduction.

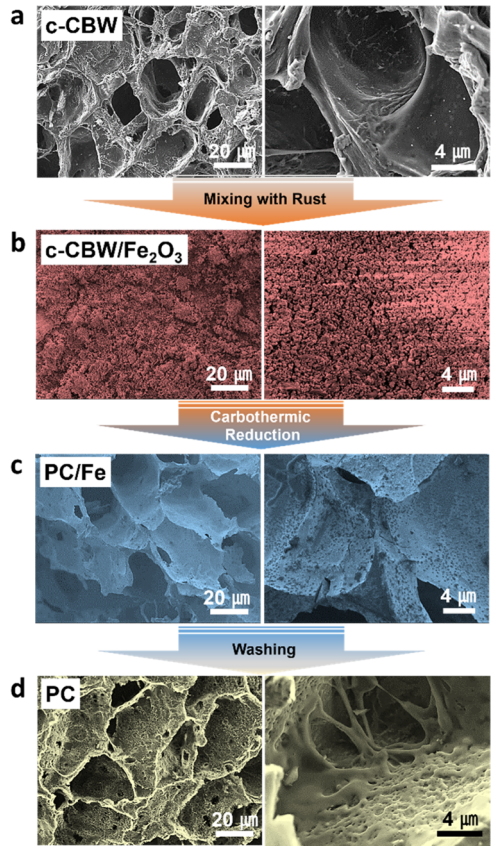

Figure 3. Morphology changes. Scanning electron microscopy (SEM) images show the morphological changes of CBW at each step of our experiment. (a) Carbonized CBW (c-CBW), (b) c-CBW mixed with iron oxide (c-CBW/Fe_2O_3), (c) porous carbon decorated with Fe particles (PC/Fe) after carbothermic reduction of c-CBW/Fe_2O_3, and (d) porous carbon after removing Fe nanoparticles by washing. It can be recognized that the surface becomes noticeably porous after carbothermic reduction. See the text for details. The initial annealing was observed to bring about less remarkable changes in the morphology of the raw CBW powder. Thus, the morphological differences between CBW and carbonized CBW (c-CBW) were less recognizable (a). The rigorous mixing with iron oxide powder with a particle size of few tens of nanometers [c-CBW/Fe_2O_3 with a weight ratio of 4(Fe_2O_3):1(CBW)] resulted in a serious change in color (from black to red) and nearly uniform coating (b). The annealing of the mixture c-CBW/Fe_2O_3 at a temperature of ∼900 °C led to significant morphological changes, likely because of the phase transformation of Fe_2O_3 that occurred during carbothermic reduction (c). The resulting porous carbon decorated with Fe particles (PC/Fe) was thinner and rougher than the CBW. After removing Fe nanoparticles by washing, the PC became even more porous (d). Regarding the elemental change and distribution of the rust (Fe_2O_3) and iron particles, further studies were performed using TEM and edx.

electron microscopy (TEM) and energy-dispersive X-ray spectroscopy (edx).

As confirmed already by the XRD results, the TEM image and selected area electron diffraction (SAED) of the c-CBW did not show any crystallinity (Figure 4a) and main components were observed to be carbon and oxygen. However, the mixture of c-CBW/Fe_2O_3 showed the existence of polycrystalline Fe_2O_3 particles with a size of few tens of nanometers (Figure 4b). The interplanar spacing of the Fe_2O_3(012) plane was measured to be ∼0.37 nm, which well corresponded with the previous XRD result (Figure 2c). After the carbothermic reduction, the Fe_2O_3 particles were observed to be fully reduced to small Fe particles, which uniformly decorated the amorphous PC matrix (Figure 4c). Some impurities (such as Ca), likely included during sample preparation, were also detected from edx. The interplanar spacing of the Fe(110) plane was measured to be ∼0.2 nm, which was also well matched up with the XRD result. After etching of PC/Fe with 1 M HCl, most of the Fe and other impurities were nearly removed and only the PC matrix with the amorphous phase remained (Figure 4d).

Magnetic Properties of Nanoporous Carbon. In order to address realizable applications of our new resources obtained from residential detritus (CBWs and rust), we gauged the magnetic properties and electrochemical performances. First, in order to verify the magnetic properties of c-CBW/Fe_2O_3 and PC/Fe, vibrating sample magnetometer (VSM) measurements were performed at room temperature. Figure 5 shows the field-dependent magnetization (M–H) curves of the c-CBW/Fe_2O_3 and PC/Fe powders together with real photographs showing response to a permanent magnet. The saturation magnetization (M_S), remanent magnetization (M_R), squareness ratio (M_R/M_S), and coercivity (H_C) values of the c-CBW/Fe_2O_3 particles were measured to be 3.23 A m^2/kg, 0.54 A m^2/kg, 0.16, and 23.1 mT, respectively. In contrast, the porous carbon decorated with nanosized Fe particles (PC/

DOI: 10.1021/acsomega.8b01280
ACS Omega 2018, 3, 7904−7910

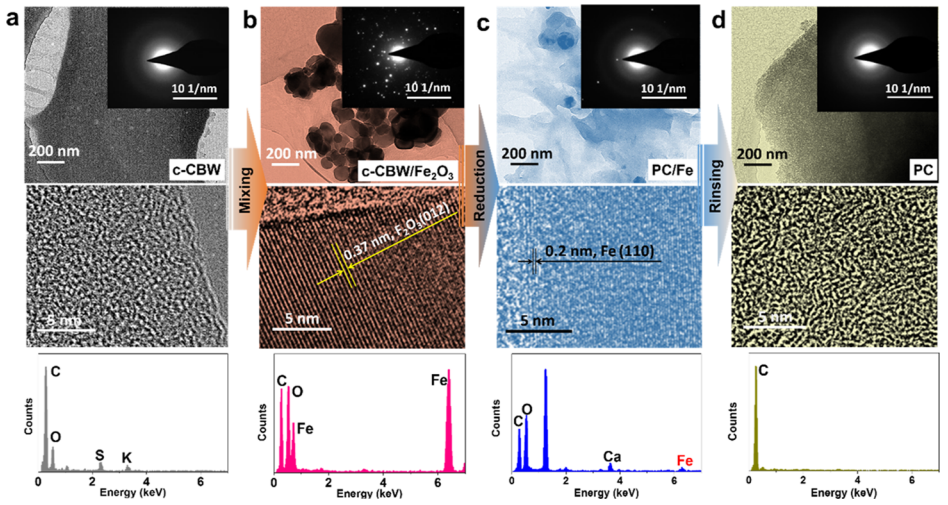

Figure 4. Microstructure study and elemental analysis. TEM, SAED, and edx analysis results of (a) carbonized CBW (c-CBW), (b) c-CBW mixed with rust (c-CBW/Fe_2O_3), (c) c-CBW/Fe_2O_3 after carbothermic reduction (PC/Fe), and (d) PC/Fe after rinsing with HCl solution (PC).

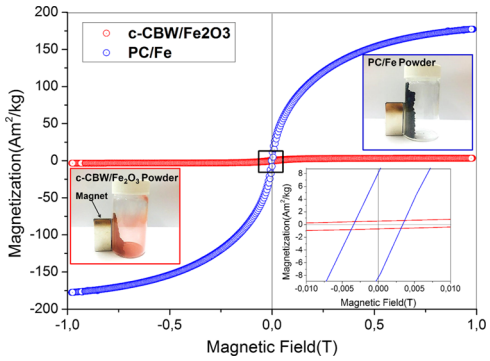

Figure 5. Magnetic properties. Magnetization hysteresis loops of the carbonized CBW mixed with Fe_2O_3 (c-CBW/Fe_2O_3) and nanoporous carbon fully decorated with ferromagnetic nanoparticles (PC/Fe). The insets show the real photographs of two kinds of powder and magnification of hysteresis.

Fe) displayed soft ferromagnetic behavior with M_S of 177.2 A m^2/kg, M_R of 7.8 A m^2/kg, and H_C of 3.3 mT. It has been reported that the M_R value of the bulk iron is around 218 A m^2/kg at room temperature.[20] Considering the report that the ferromagnetism undergoes development from atom to bulk as the size is increased,[21,22] it was a natural result that the M_S of PC/Fe is lower than that of bulk iron. Magnetic nanoparticles, thanks to size effects, such as high surface-to-volume ratio and different crystal structures, have been reported to exhibit interesting and considerably different magnetic properties than those found in their corresponding bulk materials.[20] Therefore, many types of magnetic nanoparticles, including iron oxides (e.g., Fe_3O_4 and γ-Fe_2O_3[23]), pure metal (e.g., Fe[24] and Co[25]), and alloys (e.g., $CoPt_3$[26] and FePt[27]), have been synthesized using coprecipitation, thermal decomposition, microemulsion, hydrothermal synthesis, etc.[28] Magnetic nanoparticles with proper stability have attracted great attention of environmental and biomedical application areas.[29−32] Taking into account that metallic magnetic materials such as iron, cobalt, and nickel are toxic and susceptible to oxidation, our porous carbon decorated with iron nanoparticles is likely less suitable for biomedical applications. However, encapsulation and stabilization are thought to be easily achievable by further processing. It is thought that without further processing, the PC/Fe could

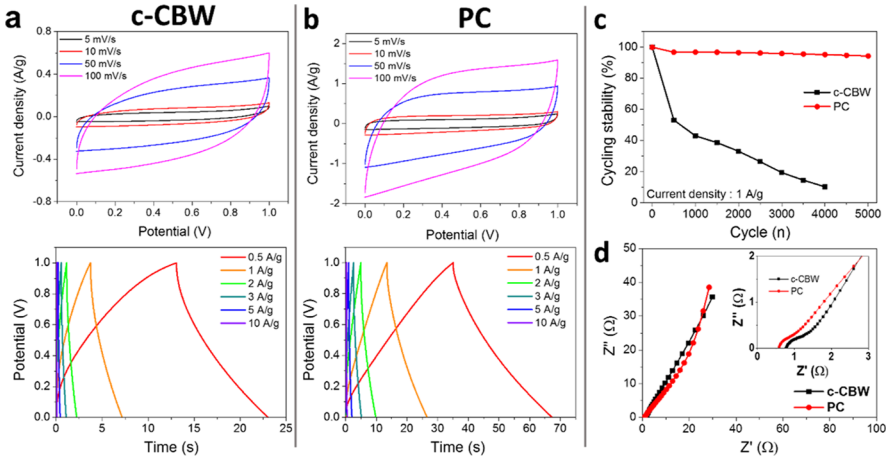

Figure 6. Electrochemical performances of two kinds of porous carbons. (a,b) CV profile at different potential scan rates and CD profile at different current densities of carbonized CBW (c-CBW) and nanoporous carbon (PC), respectively. (c,d) Cyclic stability and EIS Nyquist plot of c-CBW and PC, respectively.

DOI: 10.1021/acsomega.8b01280
ACS Omega 2018, 3, 7904−7910

be directly used in a specific applications area such as magnetic recording/storage media.[33]

Electrochemical Performances of Nanoporous Carbon. In order to address the realizable application of our PC prepared by rinsing PC/Fe with 1 M HCl, the electrochemical performance was evaluated. Numerous efforts have been put toward the utilization of the various biowastes in the energy storage sector.[34] It has been already reported that the CBWs can be employed as the precursor in fabricating supercapacitor electrodes.[35−42] In our case, we compared electrochemical performances between c-CBW prepared by simple annealing and PC prepared by carbothermic reduction. Because the surface area, evaluated by the Brunauer−Emmett−Teller (BET) method, of the PC (252.11 m^2/g) was higher than that of c-CBW (59.75 m^2/g), the electrochemical performance also showed differences. Figure 6 presents the cyclic voltammetry (CV) (current−voltage) profiles of a supercapacitor fabricated by c-CBW and PC at different potential scan rates. Both showed imperfectly rectangular CV features with a gradual change of current density with electrode polarity change. This indicated that the supercapacitor has a high internal cell resistance. The CV pattern was observed to be more resistive at higher scan rates. This type of CV profile has been typically observed in activated carbon materials produced by other synthesis methods.[43] In the CD (charge−discharge) profiles of both electrodes, the c-CBW was observed to have a lower CD time than the PC. The specific capacitance calculated from the discharge time of the c-CBW electrode was found to be quite low (7 F/g). In contrast, the PC electrode showed nearly a 4-fold increase in capacitance (27 F/g). In the case of cyclic stability (Figure 6c), the PC was maintained over 5000 cycles, whereas the c-CBW was poor. The remaining impurities such as sulfur (edx data in Figure 4a) are thought to seriously degrade the stability, likely because of the redox reaction ($S + 2H_2SO_4 \rightarrow 3SO_2 + 2H_2O$). The electrochemical impedance spectroscopy (EIS) results (Figure 6d) indicated that the PC has a slightly lower equivalent series resistance and interface resistance than the c-CBW. Although the capacitance of the PC electrode is much lower than the values reported in the literature,[35−42] it is thought that it could be surely improved via further processing or rigorous optimization.

CONCLUSIONS

In this study, we showed that the carbothermic reduction process using thermodynamic reducibility of metal oxide, typically used for metal refining, could be a simple and effective way to transform ubiquitous solid waste into a useful resource in the form of nanoporous carbon. As an example, using CBW and Fe_2O_3(rust), we produced nanoporous carbon fully decorated with magnetic nanoparticles and nanoporous carbon powder with a high surface area. Further optimization and slight modification of our process could greatly increase the material selectivity. Namely, proper combinations of carbon-based wastes and metal oxides could produce new types of resources in the form of nanomaterials, thereby likely settling economical hot potato of the conventional pyrolysis approach toward waste treatment. We hope that our method is considered as one of the ways for waste recycling using nanoscience.

EXPERIMENTAL SECTION

Preparation of Nanoporous Carbon. CBW was collected from the coffee machine installed in the library of Korea Institute of Machinery & Materials (KIMM). The collected waste was dried in an oven at 120 °C for around 24 h long. After drying, the CBW was first annealed in a quartz tube furnace under the conditions of ∼0.1 Torr and ∼800 °C for around 1 h under an Ar flow of 300 sccm. Then, the carbonized CBW (c-CBW) was mixed with Fe_2O_3. The mixing ratio between c-CBW and Fe_2O_3 was 1:4 by weight (c-CBW/Fe_2O_3). Using a planetary ball mill (BM-5L BALL-MILL, POONG LIN Co., Ltd.), the mixture was pulverized for around 12 h long at a speed of 180 rpm. Aluminum oxide balls with a diameter of 15 mm and a 250 cm^3 Teflon container were used for the ball mill. Then, the mixture (c-CBW/Fe_2O_3) was once more annealed in a quartz tube furnace under the conditions of ∼0.1 Torr and ∼900 °C for around 1 h under an Ar flow of 300 sccm. Finally, porous carbon fully decorated with iron particles (PC/Fe) was obtained. For removing Fe particles and other impurities, first of all, 1 M HCl solution was prepared, in which PC/Fe powders were immersed. The mixture was stirred at 70 °C for 1 h. Then, the mixture was filtered using a filter paper in order to obtain PC powder. Subsequently, the PC powder was rinsed using distilled water. These filtering/rinsing processes were repeated three times (Figure S3).

Preparation of an Electrode Cell. Electrodes were prepared by mixing 80 wt % activated carbon, 10 wt % carbon black, and 10 wt % polytetrafluoroethylene, with a small amount of ethanol. Each sample was fabricated into a sheet using a roll press machine. The sheet was cut into a rectangular piece of 1 × 1 cm^2 followed by heating in a vacuum oven at 80 °C. The sheet was immersed in 1 M H_2SO_4 electrolyte solution for impregnation into the pores of electrodes. After impregnation, a symmetric test cell (HS cell, Welcos Corp.) was assembled to investigate the electrochemical performances of aqueous supercapacitors, and a filter paper was used as a separator. The separator was sandwiched between the two electrodes in a test cell.

Characterizations. A field emission scanning electron microscope (JSM-7000F, JEOL) was used to analyze the surface morphology. edx was used for element analysis. XRD (Empyrean, PANalytical) was used to analyze the crystallinity of the samples. Raman spectroscopy measurements were conducted by a spectrometer (inVia Raman microscope, Renishaw) equipped with a 514 nm laser line and an objective lens (×50). TGA was conducted by TGA/DSC 1 (Mettler-Toledo instrument) at a scan rate of 10 °C/min. Specific surface areas were measured by N_2 adsorption BET (Micromeritics Tristar 3000). The TEM images were obtained using a high-resolution TEM instrument (TEM-ARM200F, JEOL) at 200 kV. The field-dependent magnetization ($M-H$) curves were measured using a VSM (Lakeshore, 7400 series). The electrochemical performances were measured with an electrochemical workstation (CHI 600E, CH instruments) with a two-electrode setup. CV and galvanostatic CD measurements were conducted. CV curves were obtained at 5, 10, 25, 50, 100, 200, 500, and 1000 mV/s with a voltage window of 1 V. Galvanostatic current was cycled at 0.5, 1, 2, 3, 5, and 10 A/g with the same voltage window. The specific capacitance C_{SP} was calculated from the CD measurements using the equation $C_{SP} = 2I/[m(dV/dt)]$, where I is the current, m is the mass of

DOI: 10.1021/acsomega.8b01280
ACS Omega 2018, 3, 7904−7910

the active material in a single electrode, and dV/dt represents the slope of the discharge curve in CD measurements.

■ ASSOCIATED CONTENT

Supporting Information

The Supporting Information is available free of charge on the ACS Publications website at DOI: 10.1021/acsomega.8b01280.

Schematic process diagram to obtain nanoporous carbon powder, Ellingham diagram of various metals (Si, Fe, Ti, and Al), and Raman and XRD analysis results of CBWs carbonized at different annealing temperatures (PDF)

■ AUTHOR INFORMATION

Corresponding Author

*E-mail: sm.lee@kimm.re.kr. Phone: +82 042 868 7659 (S.-M.L.).

Notes

The authors declare no competing financial interest.

■ ACKNOWLEDGMENTS

We would like to acknowledge the financial support from the R&D Convergence Program of MSIP (Ministry of Science, ICT and Future Planning) and NST (National Research Council of Science & Technology) of the Republic of Korea (Grant CAP-13-2-ETRI) and the Center for Advanced Meta-Materials (CAMM) funded by the Ministry of Science, ICT and Future Planning as Global Frontier Project (CAMM-nos. 2014063701, 2014063700).

■ REFERENCES

(1) Hoornweg, D.; Bhada-Tata, P. *What a Waste: A Global Review of Solid Waste Management*; The World Bank: Washington DC, 2012.

(2) Hoornweg, D.; Bhada-Tata, P.; Kennedy, C. Environment: Waste production must peak this century. *Nature* **2013**, *502*, 615−617.

(3) Czajczyńska, D.; Anguilano, L.; Ghazal, H.; Krzyżyńska, R.; Reynolds, A. J.; Spencer, N.; Jouhara, H. Potential of pyrolysis processes in the waste management sector. *Therm. Sci. Eng. Prog.* **2017**, *3*, 171−197.

(4) Nisticò, R.; Cesano, F.; Franzoso, F.; Magnacca, G.; Scarano, D.; Funes, I. G.; Carlos, L.; Parolo, M. E. From biowaste to magnet-responsive materials for water remediation from polycyclic aromatic hydrocarbons. *Chemosphere* **2018**, *202*, 686−693.

(5) Kougias, P. G.; Angelidaki, I. Biogas and its opportunities - a review. *Front. Environ. Sci. Eng.* **2018**, *12*, 14.

(6) Ma, Z.; Wang, K.; Qiu, Y.; Liu, X.; Cao, C.; Feng, Y.; Hu, P. Nitrogen and sulfur co-doped porous carbon derived from bio-waste as a promising electrocatalyst for zinc-air battery. *Energy* **2018**, *143*, 43−55.

(7) Gwak, Y. R.; Kim, Y. B.; Gwak, I. S.; Lee, S. H. Economic evaluation of synthetic ethanol production by using domestic biowastes and coal mixture. *Fuel* **2018**, *213*, 115−122.

(8) Park, S. K.; Kwon, S. H.; Lee, S. G.; Choi, M. S.; Suh, D. H.; Nakhanivej, P.; Lee, H.; Park, H. S. 10^5 cyclable pseudocapacitive na-ion storage of hierarchically structured phosphorus-incorporating nanoporous carbons in organic electrolytes. *ACS Energy Lett.* **2018**, *3*, 724−732.

(9) Park, S. K.; Lee, H.; Choi, M. S.; Suh, D. H.; Nakhanivej, P.; Park, H. S. Straightforward and controllable synthesis of heteroatom-doped carbon dots and nanoporous carbons for surface-confined energy and chemical storage. *Energy Storage Mater.* **2018**, *12*, 331−340.

(10) Liu, A.; Ren, F.; Lin, W. Y.; Wang, J. Y. A review of municipal solid waste environmental standards with a focus on incinerator residues. *Int. J. Sustainable Built Environ.* **2015**, *4*, 165−188.

(11) Ellingham, H. J. T. Reducibility of oxides and sulfides in metallurgical processes. *J. Soc. Chem. Ind., London* **1944**, *63*, 125−133.

(12) Wu, W.; Wu, Z.; Yu, T.; Jiang, C.; Kim, W.-S. Recent progress on magnetic iron oxide nanoparticles: synthesis, surface functional strategies and biomedical applications. *Sci. Technol. Adv. Mater.* **2015**, *16*, 023501.

(13) Mody, V. V.; Cox, A.; Shah, S.; Singh, A.; Bevins, W.; Parihar, H. Magnetic nanoparticle drug delivery systems for targeting tumor. *Appl. Nanosci.* **2014**, *4*, 385−392.

(14) Tang, S. C.; Lo, I. M. C. Magnetic nanoparticles: essential factors for sustainable environmental applications. *Water Res.* **2013**, *47*, 2613−2632.

(15) Jenkins, R. W.; Stageman, N. E.; Fortune, C. M.; Chuck, C. J. Effect of the type of bean, processing, and geographical location on the biodiesel produced from waste coffee grounds. *Energy Fuels* **2014**, *28*, 1166−1174.

(16) Lam, D. V.; Jo, K.; Kim, C.-H.; Kim, J.-H.; Lee, H.-J.; Lee, S.-M. Activated carbon textile via chemistry of metal extraction for supercapacitors. *ACS Nano* **2016**, *10*, 11351−11359.

(17) Lam, D. V.; Shim, H. C.; Kim, J.-H.; Lee, H.-J.; Lee, S.-M. Carbon textile decorated with pseudocapacitive VC/V_xO_y for high-performance flexible supercapacitors. *Small* **2017**, *13*, 1702702.

(18) Donskoi, E.; McElwain, D. L. S.; Wibberley, L. J. Estimation and modeling of parameters for direct reduction in iron ore/coal composites: Part II. Kinetic parameters. *Metall. Mater. Trans. B* **2003**, *34*, 255−266.

(19) Jorio, A.; Saito, R.; Dresselhaus, G.; Dressselhaus, M. S. *Raman Spectroscopy in Graphene Related Systems*, 1st ed.; Wiley-VCH: Weinheim, 2011.

(20) Huber, D. L. Synthesis, properties, and applications of iron nanoparticles. *Small* **2005**, *1*, 482−501.

(21) Billas, I. M. L.; Châtelain, A.; de Heer, W. A. Magnetism from the atom to the bulk in iron, cobalt, and nickel clusters. *Science* **1994**, *265*, 1682−1684.

(22) Tiago, M. L.; Zhou, Y.; Alemany, M. M. G.; Saad, Y.; Chelikowsky, J. R. Evolution of magnetism in iron from the atom to the bulk. *Phys. Rev. Lett.* **2006**, *97*, 147201.

(23) Sun, S.; Zeng, H. Size-controlled synthesis of magnetite nanoparticles. *J. Am. Chem. Soc.* **2002**, *124*, 8204−8205.

(24) Park, S.-J.; Kim, S.; Lee, S.; Khim, Z.; Char, K.; Hyeon, T. Synthesis and magnetic studies of uniform iron nanorods and nanospheres. *J. Am. Chem. Soc.* **2000**, *122*, 8581−8582.

(25) Puntes, V. F.; Krishnan, K. M.; Alivisatos, A. P. Colloidal nanocrystal shape and size control: the case of cobalt. *Science* **2001**, *291*, 2115−2117.

(26) Shevchenko, E. V.; Talapin, D. V.; Rogach, A. L.; Kornowski, A.; Haase, M.; Weller, H. Colloidal synthesis and self-assembly of $CoPt_3$ nanocrystals. *J. Am. Chem. Soc.* **2002**, *124*, 11480−11485.

(27) Sun, S.; Murray, C. B.; Weller, D.; Folks, L.; Moser, A. Monodisperse FePt nanoparticles and ferromagnetic FePt nanocrystal superlattices. *Science* **2000**, *287*, 1989−1992.

(28) Lu, A.-H.; Salabas, E. L.; Schüth, F. Magnetic nanoparticles: synthesis, protection, functionalization, and application. *Angew. Chem., Int. Ed.* **2007**, *46*, 1222−1244.

(29) Mohammed, L.; Gomaa, H. G.; Ragab, D.; Zhu, J. Magnetic nanoparticles for environmental and biomedical applications: A review. *Particuology* **2017**, *30*, 1−14.

(30) Issa, B.; Obaidat, I.; Albiss, B.; Haik, Y. Magnetic nanoparticles: surface effects and properties related to biomedicine applications. *Int. J. Mol. Sci.* **2013**, *14*, 21266−21305.

(31) van der Laan, G. P.; Beenackers, A. A. C. M. Kinetics and selectivity of the Fischer−Tropsch synthesis: A literature review. *Catal. Rev. Sci. Eng.* **1999**, *41*, 255−318.

(32) Pankhurst, Q. A.; Connolly, J.; Jones, S. K.; Dobson, J. Applications of magnetic nanoparticles in biomedicine. *J. Phys. D: Appl. Phys.* **2003**, *36*, R167−R181.

DOI: 10.1021/acsomega.8b01280
ACS Omega 2018, 3, 7904−7910

(33) McCurrie, R. A. *Ferromagnetic Materials Structure and Properties*; Academic Press: London, 1994.
(34) Divyashree, A.; Hegde, G. Activated carbon nanospheres derived from biowaste materials for supercapacitor applications − a review. *RSC Adv.* **2015**, *5*, 88339−88352.
(35) Yun, Y. S.; Park, M. H.; Hong, S. J.; Lee, M. E.; Park, Y. W.; Jin, H.-J. Hierarchically porous carbon nanosheets from waste coffee grounds for supercapacitors. *ACS Appl. Mater. Interfaces* **2015**, *7*, 3684−3690.
(36) Ramasahayam, S. K.; Clark, A. L.; Hicks, Z.; Viswanathan, T. Spent coffee grounds derived P, N co-doped C as electrocatalyst for supercapacitor applications. *Electrochim. Acta* **2015**, *168*, 414−422.
(37) Rufford, T. E.; Hulicova-Jurcakova, D.; Fiset, E.; Zhu, Z.; Lu, G. Q. Double-layer capacitance of waste coffee ground activated carbons in an organic electrolyte. *Electrochem. Commun.* **2009**, *11*, 974−977.
(38) Rufford, T. E.; Hulicova-Jurcakova, D.; Zhu, Z.; Lu, G. Q. Nanoporous carbon electrode from waste coffee beans for high performance supercapacitors. *Electrochem. Commun.* **2008**, *10*, 1594−1597.
(39) Wang, C.-H.; Wen, W.-C.; Hsu, H.-C.; Yao, B.-Y. High-capacitance KOH-activated nitrogen-containing porous carbon material from waste coffee grounds in supercapacitor. *Adv. Powder Technol.* **2016**, *27*, 1387−1395.
(40) Namane, A.; Mekarzia, A.; Benrachedi, K.; Belhanechebensemra, N.; Hellal, A. Determination of the adsorption capacity of activated carbon made from coffee grounds by chemical activation with ZnCl2 and H3PO4. *J. Hazard. Mater.* **2005**, *119*, 189−194.
(41) Boudrahem, F.; Soualah, A.; Aissani-Benissad, F. Pb(II) and Cd(II) removal from aqueous solutions using activated carbon developed from coffee residue activated with phosphoric acid and zinc chloride. *J. Chem. Eng. Data* **2011**, *56*, 1946−1955.
(42) Jisha, M. R.; Hwang, Y. J.; Shin, J. S.; Nahm, K. S.; Prem Kumar, T.; Karthikeyan, K.; Dhanikaivelu, N.; Kalpana, D.; Renganathan, N. G.; Stephan, A. M. Electrochemical characterization of supercapacitors based on carbons derived from coffee shells. *Mater. Chem. Phys.* **2009**, *115*, 33−39.
(43) Wang, Y.; Shi, Z.; Huang, Y.; Ma, Y.; Wang, C.; Chen, M.; Chen, Y. Supercapacitor devices based on graphene materials. *J. Phys. Chem. C* **2009**, *113*, 13103−13107.

DOI: 10.1021/acsomega.8b01280
ACS Omega 2018, 3, 7904−7910